Quantum mechanics of a classically chaotic system: Observations on scars, periodic orbits, and vibrational adiabaticity

Bruno Eckhardt and Gabriel Hose
Institut für Festkörperforschung der Kernforschungsanlage, 5170 Jülich, Federal Republic of Germany and Chemical Physics Department, Weizmann Institute of Science, Rehovot 76100, Israel

Eli Pollak
Chemical Physics Department, Weizmann Institute of Science, Rehovot 76100, Israel
(Received 26 September 1988)

We present a detailed study of the classical and quantum mechanics of a strongly chaotic quartic oscillator. The topology of the motion is such that there is a channel in which one has good separation of time scales. Many quantum states are found to scar along these channels. An adiabatic breakup for the action of the periodic orbits based on adiabatic stability of orbits is used to derive an approximate, integrable Hamiltonian. Semiclassical quantization of this Hamiltonian yields accurate energies for all states scarred along the channels.

I. INTRODUCTION

The study of quantum states and their statistical properties has received an enormous amount of attention in the past decade.[1,2] A large number of studies have focused on the statistical properties of energy levels[3–5] and have demonstrated the applicability of random matrix theory.[6–8] These results have been refined and reformulated by Berry and co-workers and today one recognizes universality classes in the level spacing distributions and rigidity of quantum states.[3,9–11]

The statistical properties of eigenvalues are intimately connected to the relationship between quantum mechanics and classical mechanics. For classically chaotic systems much effort has been guided by the Gutzwiller periodic orbit summation formula[12–17] which provides a semiclassical approximation for the quantum density of states. The recent experiments of Welge and co-workers[18–22] on the quadratic Zeeman effect and the theoretical analysis by Wintgen and Friedrich[23,24] have demonstrated that the summation formula is of practical use. The Fourier transform of the quantum density of states revealed periodicities which coincided with those of families of classical periodic orbits. It has been shown that the quantum density of states for this system can in fact be reconstructed from the periodic orbits via the summation formula.[25]

Taylor and co-workers[26] have recently demonstrated how frequencies of classical periodic orbits may appear in Fourier transforms of quantum densities of states. They note that the periodic orbits indicate classical mechanically a weak decoupling of the classical phase space from its surroundings. Therefore they suggested use of the periodic orbits to construct a quantum basis set localized around the orbits. This basis set is then used within the context of a Feshbach theory of resonances. Peaks in correlation functions are interpreted as arising from these Feshbach resonances.

Periodic orbits have appeared in a dramatic way in the studies of Heller[27,28] on the quantum eigenstates of the stadium. Heller observed that many of the quantum wave functions both at low energies and at very high energies appear to localize around the classical periodic orbits of the system. This localization has been termed as "scars" of periodic orbits. The Feshbach resonance picture[26] is consistent with the observation of scars. Bogomolny[29,30] has recently used a semiclassical expansion of the Green's function, which is similar in spirit to the derivation of the periodic orbit summation formula, in an attempt to "explain" scars.

Scars have actually been observed, prior to the study of the stadium problem, in scattering wave functions. Resonances in collinear atom-diatom collisions give rise to localization in the scattering wave function around unstable periodic orbits. This localization is actually well understood. Pollak[31] has suggested that one should distinguish between adiabatically stable and adiabatically unstable periodic orbits. An unstable orbit in the Lyapunov sense may still be adiabatically stable. Adiabatic stability is a weaker concept of stability. However, it enables the extraction of the necessary additional quantization conditions and so the prediction of resonance states. The concept of adiabatic stability has thus far not been applied to discrete bound-state systems.

The purpose of the present work is to try and obtain a somewhat better understanding of scars and their relation to classically unstable periodic orbits. To the best of our knowledge, at present, scars around unstable periodic orbits have only been observed in discontinuous systems such as the stadium. In Sec. II we report extensive numerical computations on a model two-degree-of-freedom quartic potential. A large number of converged eigenfunctions and periodic orbits have been computed. Even a cursory comparison of the two shows extensive scarring. All periodic orbits we have found are unstable in the Lyapunov sense.

In Sec. III we show that scars are formed around adiabatically stable periodic orbits. A novel method is proposed for extraction of the adiabatic frequency for motion perpendicular to the adiabatically stable periodic orbit. The method is based on the observation that an adiabatically stable orbit is usually surrounded by more complex (longer period) orbits that wind around the central orbits. These orbits may be viewed as the remnants of broken tori. The motion of these orbits may be split into a projection along and perpendicular to the path of the adiabatically stable orbit. From the perpendicular component one extracts an effective Hamiltonian for the perpendicular degree of freedom. This provides the extra quantum condition needed for prediction of quantum states. Good agreement is found between predicted energies, exact energies, and scars along the adiabatically stable orbit. Extensions and limitations of the method as well as the relationship of the method to the Gutzwiller summation formula and the Feshbach picture are discussed in Sec. IV.

II. METHODS AND RESULTS

A. The model

We chose to study the Hamiltonian

$$H=(p_x^2+p_y^2)/2+x^2y^2/2+\beta(x^4+y^4)/4 \tag{1}$$

for several reasons. The extensive numerical work of Carnegie and Percival,[32] Saviddy and co-workers,[33,34] and more recently Meyer[35] indicate that this Hamiltonian is a very strongly chaotic system, without any stable periodic orbits, in the limit $\beta\rightarrow 0$. Secondly, this Hamiltonian shows dynamical similarity because of homogeneity of both kinetic and potential energy. As a result, all periodic orbits depend trivially on energy although they do change with β. This feature implies that one can study quantum classical correspondence without worrying about bifurcations which can complicate matters enormously.[36,37]

The scaling relations between orbits at different energies are simple. A trajectory $(\mathbf{p}(t),\mathbf{q}(t))$ at energy E is determined by a trajectory $(\mathbf{p}_0(t),\mathbf{q}_0(t))$ at energy E_0 by the scaling

$$\mathbf{p}(\tau)=(E/E_0)^{1/2}\mathbf{p}_0(t),\quad \mathbf{q}(\tau)=(E/E_0)^{1/4}\mathbf{q}_0(t)\ , \tag{2}$$

where the scaled time τ satisfies

$$\tau=(E/E_0)^{-1/4}\ . \tag{3}$$

Accordingly, the classical action

$$S=\frac{1}{2\pi}\int \mathbf{p}\,d\mathbf{q} \tag{4}$$

satisfies the scaling relation

$$S(E)=S(E_0)(E/E_0)^{3/4}\ . \tag{5}$$

The ratio $\varepsilon=(E/E_0)^{3/4}$ will be referred to below as the reduced energy. The reference energy E_0 will be fixed, $E_0=\frac{1}{2}$. It is also easy to see that the integrated classical density of states $N(E)$ grows asymptotically as

$$N(E)=\int\int d\mathbf{p}\,d\mathbf{q}\,\Theta(E-H(\mathbf{p},\mathbf{q}))\approx E^{3/2}=\varepsilon^2\ . \tag{6}$$

The scaling properties also show up in the Schrödinger equation:

$$\left[-\frac{\hbar^2}{2}\Delta+x^2y^2/2+\beta(x^4+y^4)/4\right]\psi=E\psi\ . \tag{7}$$

Using the scaling $x=h^{1/3}x'$, $E=\hbar^{4/3}E'$, one finds that $\hbar$ is replaced by a value of unity in the Hamiltonian [Eq. (7)]. Thus the semiclassical limit $\hbar\rightarrow 0$ becomes equivalent to the limit $E'\rightarrow\infty$ for fixed E.

For later reference we also show the result of Gutzwiller's semiclassical analysis of the density of states. Besides a smooth term $\rho_0(\varepsilon)$ measuring the average density of states there are oscillatory contributions from periodic orbits. For our system, one finds

$$\rho(\varepsilon)=\rho_0(\varepsilon)+\sum_{\gamma}\sum_{r=1}^{\infty}|\det(1-P^r)|^{-1/2}\times\exp(i2\pi S_\gamma\varepsilon/\hbar-i\nu_\gamma\pi/2)\ , \tag{8}$$

where the summation extends over all primitive oriented periodic orbits labeled by γ, P is the 2×2 matrix of the linearization in a Poincaré surface of section perpendicular to the orbit, S_γ is the action of the periodic orbit (determined at reference energy $\varepsilon_0=1$), and ν_γ is the Maslov index of the orbit. The summation over r takes care of multiple traversals of the same orbit. A discussion of symmetry effects is given in Sec. II C.

B. Quantum states

The eigenstates of the Hamiltonian [Eq. (7)] may be classified according to the symmetry classes of the C_{4v} symmetry group. The group C_{4v} has eight elements (four reflections on the axes and the diagonals and four rotations by multiples of $\pi/2$). The irreducible representations split into four one-dimensional representations and one two-dimensional representation. In this paper we restricted ourselves to the four one-dimensional representations. These are labeled A_1 (symmetric under reflections on the axes and symmetric under reflections on the diagonals), B_1 (symmetric, antisymmetric), B_2 (antisymmetric, symmetric), and A_2 (antisymmetric, antisymmetric). This ordering corresponds to increasing energy of the ground state.

For each symmetry class the Hamiltonian was expanded in a suitable harmonic oscillator basis set and then diagonalized using standard library routines. Two modifications improved convergence considerably. First, the Hamiltonian was rotated by $\pi/4$, as seen in the figures below. This minimizes the classically forbidden region spanned by the basis set. Second, the frequency of the harmonic oscillator basis was chosen so as to minimize the trace of the matrix.[38] Since a finite basis set always provides upper bounds to the true eigenvalues, such a minimization can only improve the upper bound. Even with these improvements, we could not get a sufficient number of converged eigenvalues, let alone eigenstates for the Hamiltonian [Eq. (7)] with $\beta=0$. Therefore we

TABLE I. Scaled energies of the A_1 and B_1 states. The predicted energies in the fifth column are based on a linear approximation to the adiabatic Hamiltonian $\varepsilon_{0,m} = 0.479\,95m + 1.829\,94$. The states marked by an asterisk are in the nonlinear regime and their energies were determined by a cubic fit to the periodic orbit actions.

No.	A_1 states	No.	B_1 states	Predicted energies	Quantum numbers $m_{\|\|}$
1	1.093			1.197*	0
2	2.705	1	2.412	2.787*	2
3	3.702	2	3.587	3.808*	4
4	4.628	3	4.638	4.711*	6
5	5.478	4	5.635	5.670	8
6	5.840				
7	6.618	5	6.590	6.629	10
		6	7.110		
8	7.554	7	7.608	7.589	12
9	7.929				
10	8.516	8	8.526	8.549	14
11	8.960	9	8.969		
12	9.519	10	9.514	9.509	16
13	9.924	11	10.288		
14	10.470	12	10.526	10.469	18
15	10.816	13	11.197		
16	11.375	14	11.453	11.429	20
17	11.607	15	11.877		
18	12.366	16	12.373	12.389	22
19	12.635	17	12.776		
20	12.820				
21	13.347	18	13.345	13.349	24
22	13.469	19	13.602		
23	14.033	20	14.084		
24	14.318	21	14.322	14.309	26
25	14.690	22	14.757		
26	15.012				
27	15.288	23	15.262	15.269	28
		24	15.346		
28	15.849	25	15.837		
29	16.015	26	16.025		
30	16.257	27	16.264	16.228	30
31	16.594	28	16.890		
32	17.044				
33	17.216	29	17.153	17.188	32
34	17.350	30	17.292		
35	17.805	31	17.713		
36	18.080	32	18.096	18.148	34
37	18.242	33	18.274		
38	18.607	34	18.769		
39	18.933	35	18.848		
40	19.127	36	19.092	19.108	36
41	19.432	37	19.317		
42	19.660	38	19.819		
43	19.974	39	19.987		
44	20.143	40	20.165	20.068	38
45	20.524	41	20.570		
46	20.868	42	20.739		
47	20.987	43	20.980	21.028	40
48	21.202	44	21.204		
49	21.274	45	21.547		
50	21.679				
51	21.922	46	21.940	21.988	42
52	22.012	47	22.136		
53	22.267	48	22.344		
54	22.644	50	22.398		

TABLE I. (*Continued*).

No.	A_1 states	No.	B_1 states	Predicted energies	Quantum numbers $m_{\|}$
		51	22.883		
55	22.907	52	22.960	22.948	44
56	23.057	53	23.273		
57	23.275	54	23.350		
58	23.567				
59	23.730	55	23.842		
60	23.875	56	23.893	23.908	46

chose to cut off the channels along the axes (the main feature responsible for "spoiling" convergence) by fixing β at 0.01.

High-accuracy solutions for the eigenvalues were obtained using 79 (for the A_1 and B_1 states) or 80 (for B_2 and A_2) harmonic eigenstates for each degree of freedom, resulting in matrices of dimension 3240. For the plots of the eigenfunctions, smaller matrices were used (size <1000) but we made sure that changes remained marginal. The first 60 eigenvalues for the symmetry classes A_1, B_1, B_2, and A_2 are tabulated in Tables I and II. All these eigenvalues are converged to within five significant figures.

The densities ($|\psi|^2$) of the first 60 eigenfunctions for the A_1 symmetry class are plotted in Fig. 1. (Deviations between the numbers given in the table and the eigenvalues listed with the eigenfunctions are due to basis sets of different size and are thus a measure of convergence.) Here we have rotated the potential energy contour by $\pi/4$ so that the (x,y) coordinates lie along the diagonals. The densities of the first 24 eigenfunctions for each of the other symmetries are plotted in Figs. 2–4, respectively. In these plots there are some obvious properties associated with the respective symmetries. For the A_1 symmetry there are no nodal lines on the axes or the diagonals. The B_1 states have nodal lines along the axes, the B_2 states along the diagonals, and the A_2 states along the axes and the diagonals. Beyond these symmetries, it is obvious that many of the wave functions are localized in configuration space, in contrast to what might be expected from a classical microcanonical distribution. By studying the periodic orbits of the system we will see that these localizations are scars of unstable periodic orbits.

In Fig. 5 we plot the Fourier transform of the quantal spectra for the A_1 states. Here the Fourier transform is in reduced space and defined as

$$C(s)=\left|\int_{-\infty}^{\infty} d\varepsilon\, e^{2\pi i s\varepsilon}\rho(\varepsilon)\right|^2=\left|\sum_n e^{2\pi i s\varepsilon_n}\right|^2, \tag{9}$$

where $\rho(\varepsilon)$ is the quantal density of states, ε_n are the (reduced) eigenvalues, and we did not subtract the classical average since it would make little difference with the relatively few states involved in the summation. The "time" variable s has the dimensions of an action. From the figure one can resolve some very distinct peaks. In the next section we will show, as one might expect on the basis of Eq. (8), that many of these peaks may be identified with the action of a periodic orbit whose instability is relatively weak. This result is identical to a similar analysis of quantum states of Wintgen and Friedrich.[23,24]

C. Periodic orbits

The Hamiltonian used is given in Eq. (1) with $\beta=0.01$. As shall be shown shortly, all periodic orbits we could find for this choice were unstable. Poincaré surfaces of sections (an example is shown in Fig. 6) were space filling and configuration space plots of trajectories integrated for very long times gave uniform distributions in configuration space. These attributes indicate classical mechanical chaos.

A practical method for obtaining all periodic orbits whose period is less than some predetermined time T is not available. A search for all periodic orbits involves in principle a multidimensional search in a Poincaré surface of section. However, substituting completeness for efficiency, it is possible to locate many orbits by searches along symmetry lines.[39] For the Hamiltonian at hand there are three immediate such lines; the coordinate axes, the diagonals, and the boundary of the classically allowed configuration space at energy E. For the first two cases, one initiates trajectories perpendicular to the symmetry line and searches for perpendicular intersections after a given number of crossings using interval bisections. For orbits initiated along the boundary we used the turning-point method of Ref. 40 which is also implemented with interval bisections.

The actions and periods of the orbits are not very sensitive to the accuracy of determination of the orbit. However, the eigenvalues obtained from a linear stability analysis are very sensitive to the accuracy in determining the precise period of the orbit. We therefore used an idea suggested by Hénon[41] which enables numerical integration exactly to the point where the stopping condition is met. In this manner, the accuracy is determined solely by the number of interval bisections used. We could converge eigenvalues up to modulus of about 10^4.

Altogether a total of 150 periodic orbits were computed, not counting symmetries or multiple traversals. In order to analyze quantum states with the aid of periodic orbits it is necessary to consider the role of symmetry. As mentioned, the quantum states are symmetrized according to the group elementss of C_{4v}. The orbits too

TABLE II. Scaled energies of the B_2 and A_2 states. The predicted energies in the fifth column are based on a linear approximation to the adiabatic Hamiltonian $\varepsilon_{1,m} = 0.479\,95m + 5.009\,88$. The states marked by an asterisk are in the nonlinear regime and their energies were determined by a cubic fit to the periodic orbit actions.

No.	B_2 states	No.	A_2 states	Predicted energies	Quantum numbers $m_{\|}$
1	3.367			3.592*	1
2	5.390	1	4.848	5.495*	3
3	6.493	2	6.407	7.044*	5
4	7.436	3	7.656	8.362*	7
5	8.166				
6	8.814	4	8.712	9.502*	9
		5	9.312		
7	9.787	6	9.920	10.506*	11
8	10.401				
9	10.785	7	10.833	11.423*	13
10	11.319	8	11.422		
11	11.935	9	11.921	12.309*	15
12	12.352	10	12.686		
13	12.904	11	13.070	13.205*	17
14	13.409	12	13.498		
15	13.813	13	13.913	14.132*	19
16	14.214	14	14.514		
17	14.845	15	14.873	15.089	21
18	15.125	16	15.375		
19	15.290				
20	15.898	17	15.912	16.049	23
21	16.037	18	16.183		
22	16.657	19	16.606		
23	16.957	20	16.961	17.009	25
24	17.126	21	17.285		
25	17.685	22	17.788		
26	17.983	23	18.049	17.969	27
27	18.480	24	18.271		
28	18.572	25	18.696		
29	18.882	26	18.999	18.928	29
30	19.346	27	19.639		
31	19.422	28	19.715		
32	19.744	29	19.966	19.888	31
33	20.177				
34	20.444	30	20.394		
35	20.733	31	20.724	20.848	33
36	21.067	32	20.988		
37	21.148	33	21.350		
38	21.684	34	21.402		
39	21.738	35	21.738	21.808	35
40	22.103	36	22.148		
41	22.368	37	22.370		
42	22.725	38	22.730	22.768	37
43	22.793	39	22.959		
44	23.268	40	23.067		
45	23.388	41	23.513		
46	23.690	42	23.726	23.728	39
47	23.849	43	23.949		
48	24.019	44	24.374		
49	24.176	45	24.680		
50	24.656	46	24.718	24.688	41
51	24.838	47	25.001		
52	25.037	48	25.196		
53	25.366	49	25.421		
54	25.659	50	25.666	25.648	43
55	25.820	51	25.965		

TABLE II. (*Continued*).

No.	B_2 states	No.	A_2 states	Predicted energies	Quantum numbers $m_{\|}$
56	25.904	52	26.160		
57	26.291				
58	26.448	53	26.480	26.608	45
59	26.639	54	26.653		
60	26.832	55	26.808		

can be invariant under some symmetry operations. This affects their contribution to either an adiabatic approximation or to the semiclassical expansion (8) and thus also the analysis of the Fourier transform of the A_1 states shown in Fig. 5. In particular, the periodic orbit expansion extends over periodic orbits that are different in *phase space*. The summation must take into account the symmetries of the equations of motion in phase space. In our system, there are eight geometrical symmetries to the potential and time-reversal symmetry, making for a total of 16 symmetries in phase space. (The geometric symmetries are extended to act on momenta as well.) We will say an orbit is invariant under one of the symmetries, if the set of points in phase space belonging to the orbit is mapped into itself (preserving the orientation where applicable). By inspection one then finds the following possibilities.

The only orbits invariant under time-reversal symmetry are those that have two points on the equienergy contour. As a result, these orbits usually have only twofold geometrical symmetries, i.e., invariance under rotation by π as for orbit 1 in Fig. 7(a) or invariance under a reflection as for orbit 25. Any higher symmetry would imply four points along the equienergy contour which is impossible unless the orbit itself runs along a symmetry line (nos. 2 and 9). On the other hand, an orbit in this class may have no other symmetry at all, as, e.g., orbits 52,3,11,38,46, . . . in Fig. 7(b). Thus self-retracing orbits belong to groups of eight (no geometrical symmetry), four (one geometrical symmetry), or two (orbits along symmetry lines) degenerate periodic orbits.

Orbits without time-reversal symmetry exist at least in pairs. If the orbit does not have any geometrical symmetries, then it comes in 16 copies, 8 geometrical ones traversed in two directions each. Our methods of search are incapable of finding these orbits, though we did establish that they exist by finding one using two-dimensional a ($2D$) Newton method.

There are orbits that do have at least a twofold geometrical symmetry [such as nos. 24,7,48, . . . in Figs. 7(a) and 7(b)]. However, if the geometrical symmetry is a reflection then it needs to be combined with time reversal; for instance, for orbit 7 the symmetry is reflection along the diagonal plus time reversal. These orbits then belong to groups of eight twofold-degenerate orbits. If the symmetries of the orbit are higher, then the number of copies is decreased correspondingly. If the orbit has a four-dimensional symmetry, then it belongs to a group of four fourfold-degenerate orbits. Again some of the symmetries can be combinations of time-reversal and geometrical symmetries. The most symmetrical orbits are invariant under a group with eight symmetry elements and thus belong to a pair of eightfold-degenerate orbits [like nos. 13 and 32 in Fig. 7(c)]. This exhausts all possibilities: orbits come in groups of eightfold- (no geometrical symmetry), fourfold- (one geometrical symmetry), or twofold-degenerate periodic orbits. (The case of a single orbit invariant under all 16 symmetry operations is excluded since it would have to be self-retracing.)

With this knowledge we can analyze their contribution to the expansion (8) via a symmetrization of the Green's function as outlined by Gutzwiller.[16,17] Obviously, the Green's function of the full quantum problem can be written as a sum over Green's functions for the individual irreducible representations,

$$G(\mathbf{x},\mathbf{y})=\sum_s G_s(\mathbf{x},\mathbf{y}) , \tag{10}$$

where $s\in\{A_1,B_1,B_2,A_2,E\}$. Each one has the usual representation in terms of the eigenstates of that symmetry class:

$$G_s(\mathbf{x},\mathbf{y})=\sum_n \frac{\psi_n^s(\mathbf{x})\psi_n^s(\mathbf{y})}{E-E_n} . \tag{11}$$

Applying a symmetry operation P to one of the arguments of the reduced Green's functions changes the sign of one of the wave functions according to the character of the group element. One can thus obtain the symmetry reduced Green's functions from the full Green's functions by suitable sums and differences of G for different arguments.

In the semiclassical approximation, the Green's function contains contributions from all *oriented* classical paths from $\mathbf{x}$ to $\mathbf{y}$. If the initial and final points lie on a periodic orbit that has symmetries preserving its orientation, then this orbit will not only contribute to the Green's function from $\mathbf{x}$ to $\mathbf{y}$, but also to that from $\mathbf{x}$ to $P\mathbf{y}$, where P stands for the symmetry operation. Specifically, let us consider orbit 23 and its contributions to the Green's function of the A_1 symmetry class. As indicated in Fig. 8, points b', b'', and b''' are symmetry related to point b. Their contribution to G_{A_1} is

$$G(a,b)+G(a,b')+G(a,b'')+G(a,b''') . \tag{12}$$

In the semiclassical limit, the Green's function is represented by[42]

$$G(a,b)\approx A_{a,b}e^{i2\pi S_{a,b}/\hbar+i\nu\pi/2} , \tag{13}$$

where $S_{a,b}$ is the classical action, ν the Maslov index for this piece of trajectory, and the amplitude $A_{a,b}$ is given by $(\partial S_{a,b}/\partial a \partial b)^{1/2}$. It is easy to derive the relations

$$S_{a,b''}=S(T/2)+S_{a,b} , \tag{14a}$$

$$S_{a,b'''}=S(T/2)+S_{a,b'} \tag{14b}$$

for the actions. The Maslov index for a trajectory piece shorter than half a period is 0, since one can always find a representation where there are no conjugate points. If the segment is longer, than the Maslov index is 2, as it picks up all the conjugate points. Thus Eq. (12) can be rewritten

$$(1+e^{i2\pi S(T/2)/\hbar+\pi})[G(a,b)+G(a,b')] . \tag{15}$$

TABLE III. Periodic orbits for the classical Hamiltonian (2.1) with $\beta=0.01$ and $E_0=\frac{1}{2}$, ordered by increasing instability.

No.	Period	Action	u	$S_{\parallel}$	$S_{\perp}$
1	19.6745	2.0875	1.29	1.8891	0.0283
2	19.7210	2.0925	1.68	2.0925	0.0000
3	10.7592	1.1416	3.94	0.6215	0.2600
4	17.6663	1.8745	4.07	1.3704	0.1008
5	8.2891	0.8795	4.20	0.4397	0.4397
6	19.2169	2.0390	4.44	1.6408	0.0663
7	8.0462	0.8537	4.60	0.7378	0.0579
8	39.3603	4.1763	4.70	1.9361	0.0217
9	7.3979	0.7849	4.77	0.3925	0.3925
10	19.4407	2.0627	5.23	1.6427	0.0700
11	10.6287	1.1277	5.25	0.5948	0.2664
12	23.2413	2.4660	5.43	0.7095	0.2094
13	9.3264	0.9896	5.58	0.4948	0.4948
14	19.0585	2.0222	5.83	1.4650	0.0928
15	16.2050	1.7194	6.01	1.1257	0.1484
16	14.0882	1.4948	6.05	0.8845	0.2034
17	18.7857	1.9932	6.07	0.5153	0.3209
18	17.6194	1.8695	6.10	1.2445	0.1250
19	18.3031	1.9420	6.29	1.3363	0.1211
20	12.3195	1.3071	6.48	0.6877	0.3097
21	59.0386	6.2642	6.64	1.9448	0.0205
22	18.5181	1.9648	6.68	1.3087	0.1312
23	11.3391	1.2031	6.72	0.6162	0.2935
24	13.7570	1.4597	6.86	0.8021	0.2192
25	12.7114	1.3487	6.92	0.6990	0.3248
26	59.0736	6.2679	6.94	1.9833	0.0151
27	15.9764	1.6951	7.00	1.0017	0.1733
28	16.8774	1.7907	7.02	1.0876	0.1758
29	17.8905	1.8982	7.03	1.1911	0.1414
30	14.9309	1.5842	7.09	0.8831	0.2337
31	39.2228	4.1617	7.11	1.8530	0.0351
32	22.2993	2.3660	7.20	0.3943	0.3943
33	17.0924	1.8136	7.29	1.0734	0.1850
34	15.1863	1.6113	7.37	0.8806	0.2436
35	16.2501	1.7242	7.48	0.9821	0.1855
36	16.0705	1.7051	7.62	0.4294	0.4231
37	25.0201	2.6547	7.63	0.8158	0.1705
38	19.0658	2.0229	7.81	0.5301	0.3209
39	38.3707	4.0713	8.01	1.6461	0.0649
40	21.0885	2.2376	8.28	0.6645	0.2271
41	39.1609	4.1551	8.31	1.7576	0.0492
42	58.8291	6.2420	8.33	1.8112	0.0404
43	15.9036	1.6874	8.59	0.4224	0.4213
44	58.9527	6.2551	8.65	1.9316	0.0230
45	29.2439	3.1029	8.76	0.9811	0.1630
46	19.0224	2.0183	8.75	0.5227	0.3243
47	20.9747	2.2255	8.76	0.6143	0.2492
49	16.3201	1.7316	8.84	0.7615	0.0521
49	27.5799	2.9263	9.05	0.9165	0.1822
50	58.8293	6.2420	9.10	1.8219	0.0388

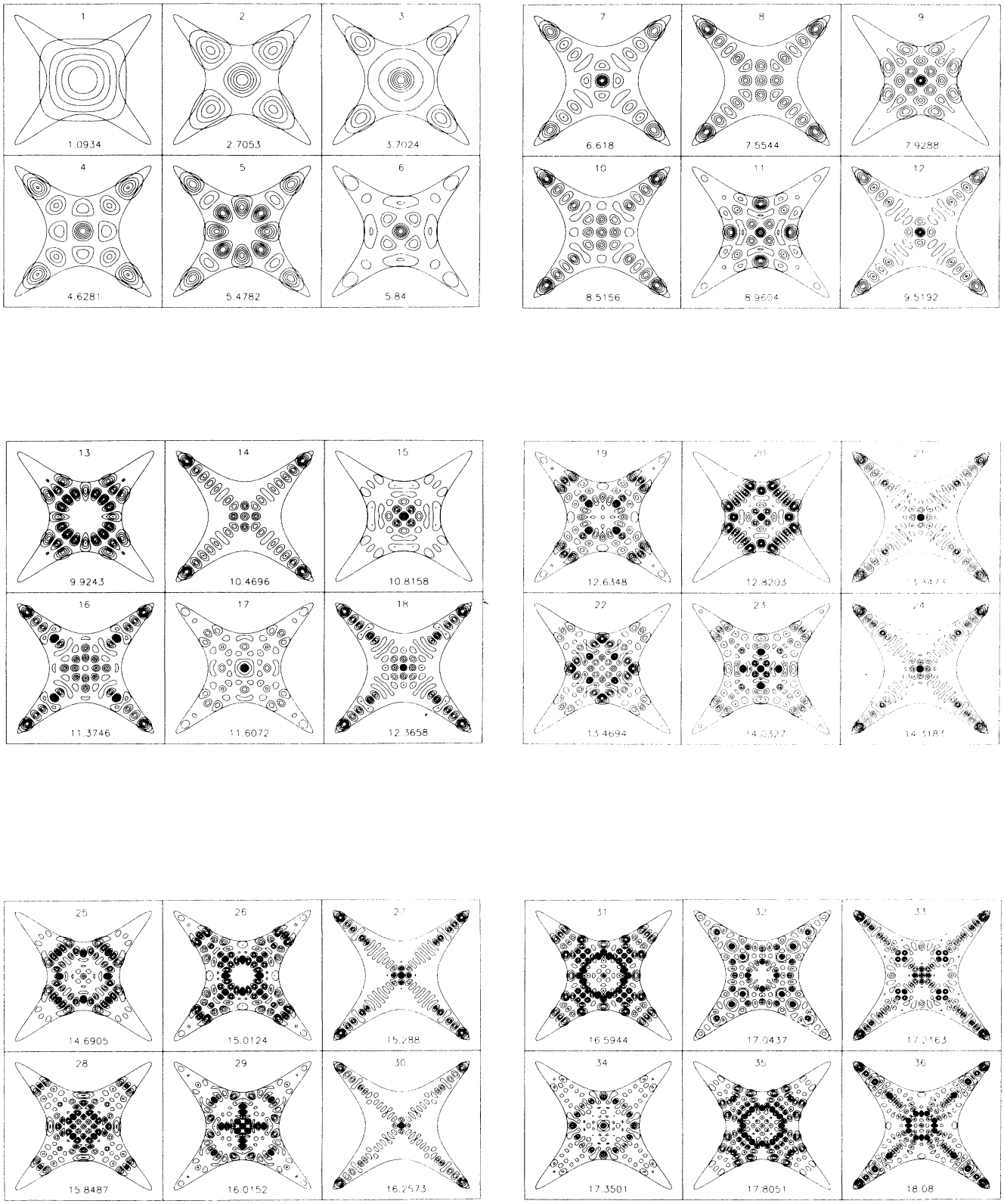

FIG. 1. Densities $|\psi|^2$ of the lowest 60 eigenstates in the symmetry class A_1. In each panel the upper number is the number of the eigenstate and the lower number is the scaled energy.

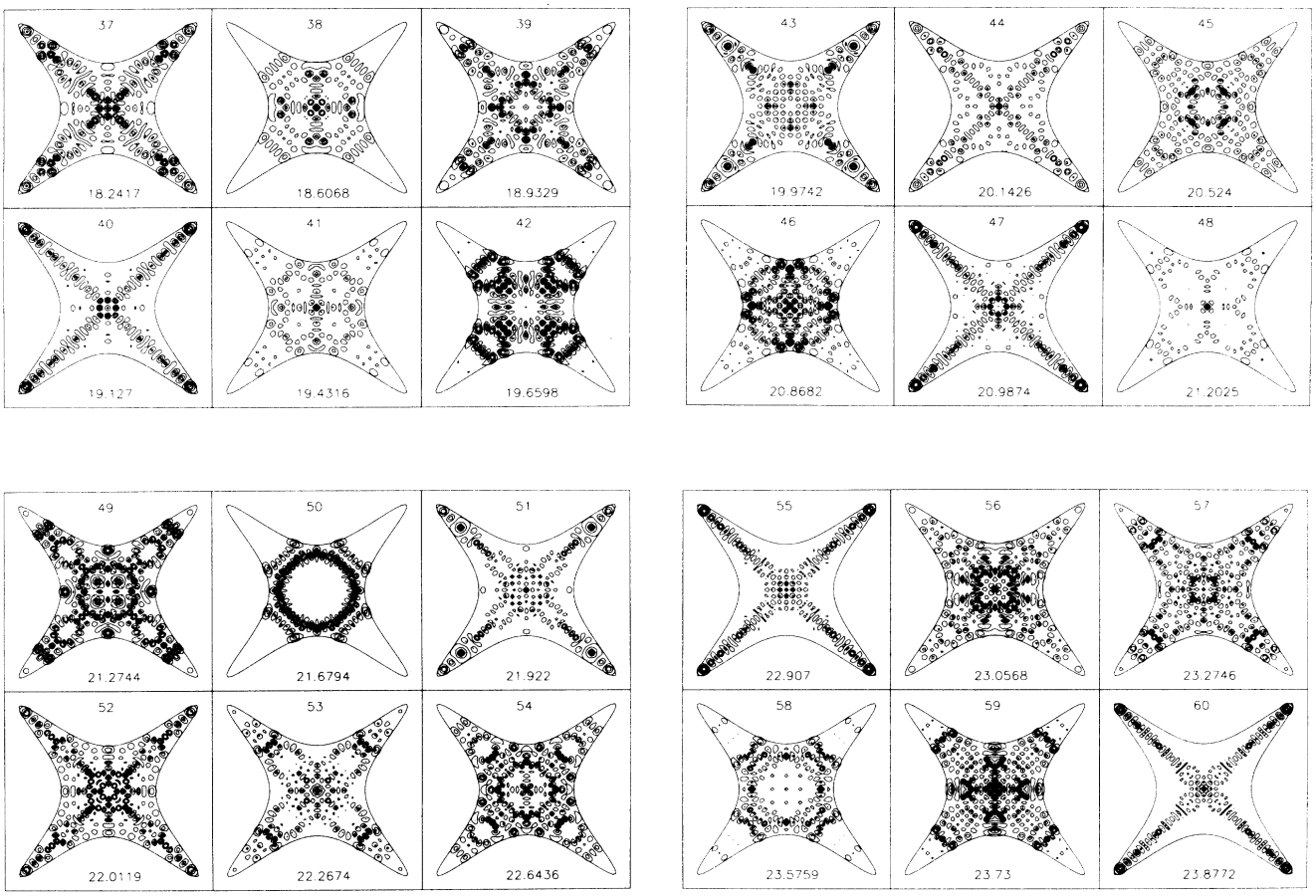

FIG. 1. (*Continued*).

The first term vanishes, if $S(T/2)=(n+\frac{1}{4})\hbar$ or $S(T)=(2n+1/2)\hbar$. Analysis of the second term shows that it vanishes for n even. Thus the (full) action is quantized in units of $4\hbar$. This is the same as saying that within a given symmetry subspace one has integer quantization of one-quarter the action. It is this symmetry reduced action that will appear in the Fourier transform of the density of states [Eq. (9)].

This type of analysis can be repeated for the other orbits as well. One finds that self-retracing orbits contribute either with the full action (no geometrical symmetries) or with half action (one geometrical symmetry or along symmetry lines) and that non-self-retracing orbits contribute with action divided by degeneracy.

Besides this rather cumbersome group-theoretical argument there is also a more intuitive one based on "standing waves along the orbit." By this we mean the following. Introduce a coordinate system along the orbit and disregard the perpendicular motion. In this coordinate system the motion is either a libration (if the orbit is self-retracing) or a rotation. Symmetries of the orbit also show up in this coordinate system and one can argue by one-dimensional analogy. For instance, the motion of orbit 2 is a libration with reflection symmetry, so that one-dimensional states with even quantum numbers will correspond to symmetric standing waves, whereas states with odd quantum numbers correspond to antisymmetric waves. Again the spacings between consecutive energies in one symmetry class are the same as if the periodic orbit had only half the action. A similar argument applies to the rotation of periodic orbits like no. 13 or 32. Perpendicular excitations do not change this picture.

We should point out that the symmetries of the orbit also affect the stability exponents that enter the periodic orbit formula. For instance, an orbit hyperbolic after a full period may be inverse hyperbolic after half a period. For further discussion of this point see Refs. 43 and 25.

In Table III we provide the (full) actions of the 50 least unstable periodic orbits (this list is not exhaustive, considering the limitations of our search). We also list u, the logarithm of the maximal eigenvalue of the linearization in a Poincaré surface of section perpendicular to the orbit. The amplitudes in the periodic orbit formula are then given by $[\sinh(ur/2)]^{-1/2}$ or $[\cosh(ur/2)]^{-1/2}$ [r is the number of traversals of the orbit, see Eq. (9)], if the full orbit contributes and if it is hyperbolic or inverse hyperbolic, respectively.

In Fig. 7 we show a few selected orbits. All orbits in Fig. 7(a) move "in the channel," that is, they are confined to an elongated region excluding the second channel. The first two are the least unstable orbits found by our method. For later purposes we note that orbit 1 can be

decomposed into one oscillation along the long axis and seven oscillations perpendicular to it. Similarly, nos. 8 and 21 correspond to two oscillations along the long axis and 14 and 15 oscillations perpendicular to the axis, respectively. The orbits in the second row seem to belong to a family of periodic orbits with four, six, eight, ten, etc. crossings of the long axis. Similarly, the bottom row also suggests a family of orbits crossing the origin with again a total of four, six, eight, etc. crossings of the long axis. These symmetrical orbits can also occur in integrable systems (see the discussion by Berry and Tabor[44,45]). However, orbit 24 in the last panel of Fig. 7(a) indicates that a family of asymmetric orbits also exits. One can imagine a symbolic organization of these orbits by the number of crossings of the channel axes left and right of the center.

Figure 7(b) shows orbits that stay mainly in the central region of configuration space. From these sets one can identify some "basic orbits," namely nos. 5, 9, 3, and 11. All the other orbits shown can be "projected" onto these basis ones. For instance, no. 7 is roughly half a period of no. 9 closed by half a period of no. 5. Orbit no. 48 may be decomposed as either one period of no. 5 and one period of no. 7 or half a period of no. 9 and $\frac{3}{2}$ periods of no. 5. The symmetry-related orbits can also be connected in this fashion, see nos. 57, 58, and 121. The existence of these concatenated orbits follows from the theory of chaos in dynamical systems: If the system is completely chaotic, i.e., all periodic orbits are unstable, then their stable and unstable manifolds intersect in heteroclinic points. One intersection immediately implies infinitely many. The heteroclinic points belong to trajectories that start asymptotically in the far past near one orbit and end in the far future near another. It is now conceivable that nearby there are periodic orbits mimicking this motion for some time. A good example is no. 48. Finally, in Fig. 7(c) we show two highly symmetric orbits (nos. 13 and 32) as well as some more complicated (heteroclinic) orbits between all four motions.

A cursory comparison of the orbits in Fig. 7 with the wave functions plotted in Figs. 1–4 shows that many of the wave functions may be thought of as having scars of unstable periodic orbits. Some of these scars will be analyzed in detail in the next section. This point is further stressed by inspection of Fig. 9. Here we plot the actions of the orbits (as they contribute to the density of states)

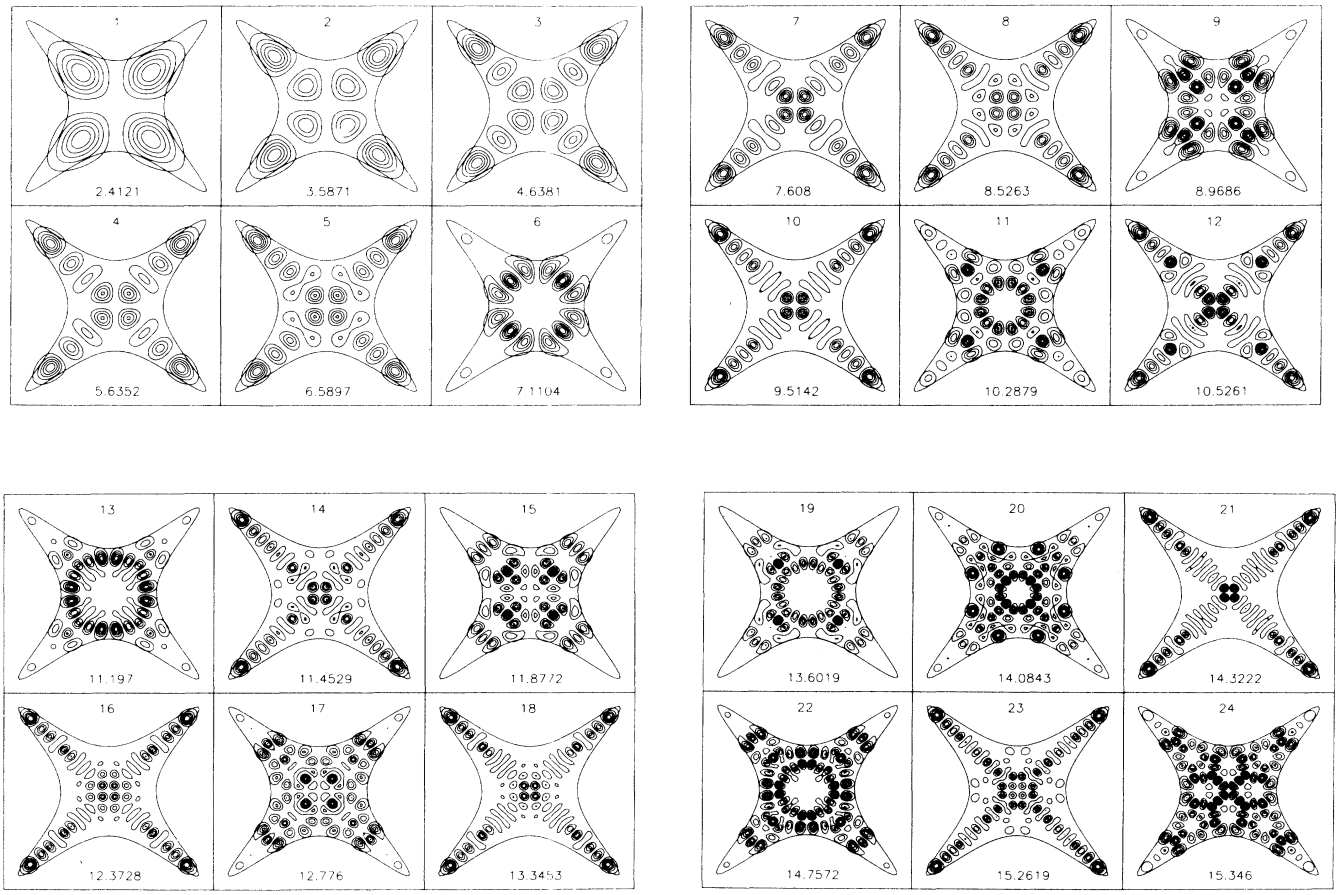

FIG. 2. Densities of the lowest 24 eigenstates in the symmetry class B_1.

versus their characteristic exponents [ordinary and inverse hyperbolic points are not distinguished since the differences in amplitude in (8) are small]. Comparison of this figure and the prominent peaks (at $s=1.04, 2.08, \ldots$) observed in the Fourier transform of the density (Fig. 5) shows that these peaks may be correlated with the actions of the two least unstable periodic orbits. These same orbits appear as scars in many of the wave functions, however, the Fourier transform and the scars are not sufficient for distinguishing between the two. Clearly, there are additional peaks in the Fourier transform and it is not difficult to find orbits whose actions or multiples thereof lie in the desired range. It is impossible though to provide unambiguous correlations for any action greater than about 0.6 (from the orbits we computed, 13 have symmetry reduced actions less than 0.8 and another 19 have actions between 0.8 and 1.04, the action of the least unstable periodic orbit).

III. VIBRATIONAL ADIABATICITY

The purpose of this section is to show that scars of wave functions around unstable periodic orbits may arise as a result of the adiabatic stability of the unstable (in the sense of Lyapunov) periodic orbit (henceforth PO). To show this it is first necessary to review the notion of adiabatic stability and understand the relevance of this concept to quantum mechanics. Linear stability analysis gives properties of the orbits associated with behavior at infinite time. When one finds that a periodic orbit is unstable in the Lyapunov sense, one really means that if one waits long enough an orbit in the neighborhood of the PO will find itself an arbitrary large distance away from the PO. This does not preclude the possibility that for short times, for example, times of the order of the period of the PO itself, a neighboring trajectory will remain in the neighborhood of the orbit. An analysis of semiclassical quantization shows that roughly it suffices to stay in the vicinity of a PO one period for quantum effects to become important.[46] In other words, for quantum mechanics it is the short-time behavior of the orbit which is really important.

It has been noted[40] that periodic orbits can be characterized as repulsive or attractive based on the short-time behavior of trajectories in their neighborhood. A repulsive orbit is one such that any trajectory in its neighborhood will move away from the PO. An attractive orbit is one such that any orbit in its neighborhood will cross it before completing one cycle along the orbit. Examples for the quartic potential are shown in Fig. 10. An orbit

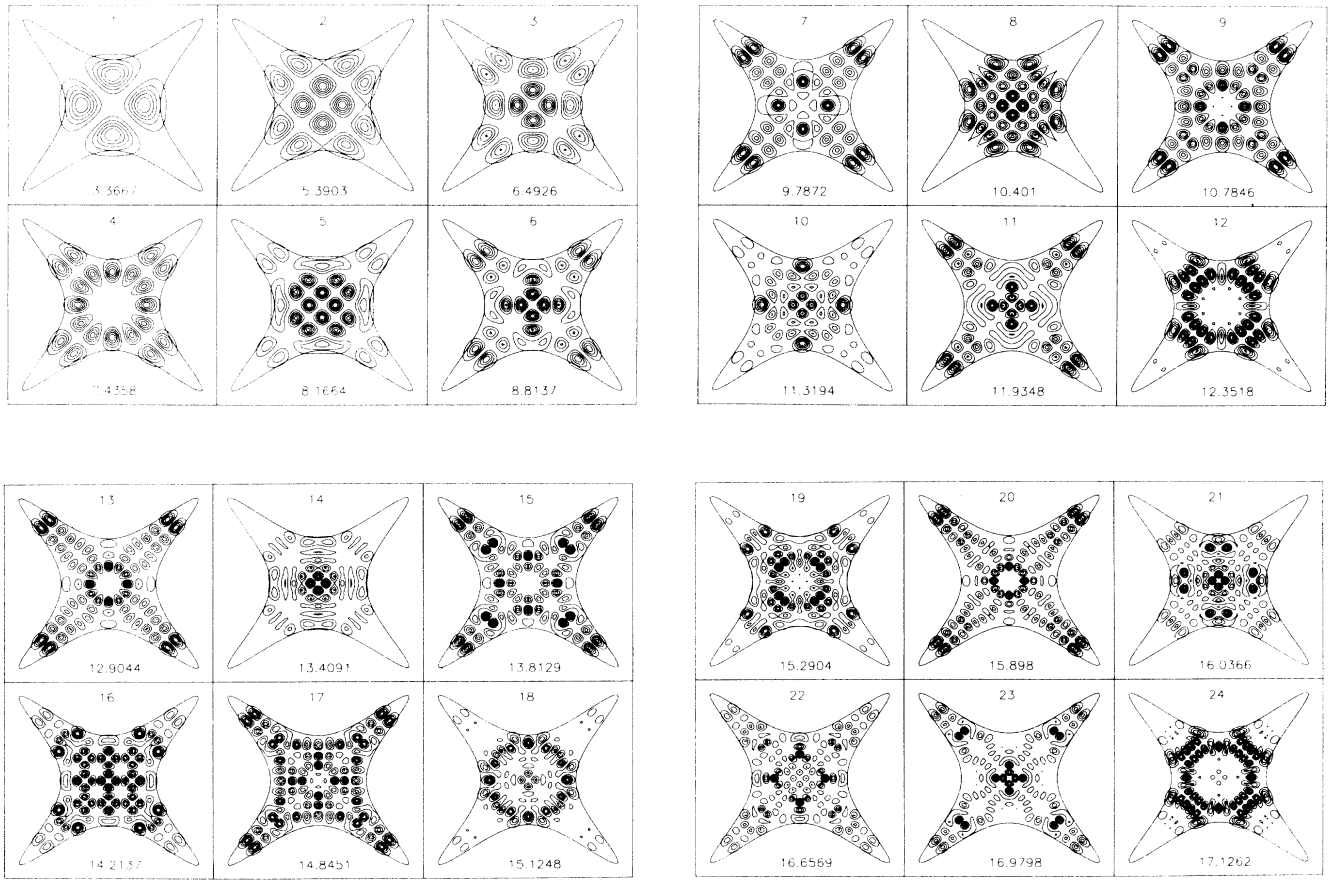

FIG. 3. Densities of the lowest 24 eigenstates in the symmetry class B_2.

can be simultaneously attractive and unstable in the Lyapunov sense.

Consider now the approximation of vibrational adiabaticity. A necessary condition for the vibrationally adiabatic approximation to be exact is that the barriers and wells on the vibrationally adiabatic surface are periodic orbits.[31,47,48] At an adiabatic barrier, neighboring trajectories will move away from the orbit as in Fig. 10(a). At a well, if the adiabatic approximation is to make any sense, trajectories will move toward the orbit as in Fig. 10(b). Thus, by inspection alone, one can categorize a PO as an adiabatic barrier or well simply by the behavior of nearby trajectories, that is, by the repulsive or attractive characteristic.

If the adiabatic approximation around an orbit is exact and the orbit is a well then motion around the orbit is integrable and the orbit must be stable in the sense of Lyapunov. Any orbit in its vicinity may be described (in a two-degree-of-freedom system) by the action along the direction of the central orbit ($S_{\parallel}$) and the perpendicular action ($S_{\perp}$). These two actions are by construction constants of the motion. Any orbit in the vicinity, with the same $S_{\parallel}$ and finite $S_{\perp}$ must by construction be at an energy higher than that of the PO. In other words, the action of the adiabatic well is a local maximum. Similarly it is easy to convince oneself that around an adiabatic barrier, the action of the PO is a local minimum.

If the adiabatic approximation is not exact then motion around the orbit is no longer integrable and the orbit is unstable in the Lyapunov sense. It is still possible though to define an adiabatic approximation in its vicinity. Specifically, one constructs a local orthogonal coordinate system which coincides along a line with the PO. If the orbit is an adiabatic well it will retain the maximum property with respect to the action ($S_{\parallel}$). In other words, adiabatic wells are identified by their attractive behavior and by the fact that their action must be in some sense a local maximum.

Before proceeding to the practical aspects we note that if the Lyapunov exponent of the attractive PO is not too large, the adiabatic approximation can be expected to be reasonably accurate for a finite time and so one can expect that a semiclassical quantization based on the adiabatic breakup will give reasonable estimates for the eigenvalues. It has been shown by several authors that in the stadium problem,[49,50] certain states may be approximated reasonably well by an adiabatic breakup. The main thrust of the present discussion is to show how the adia-

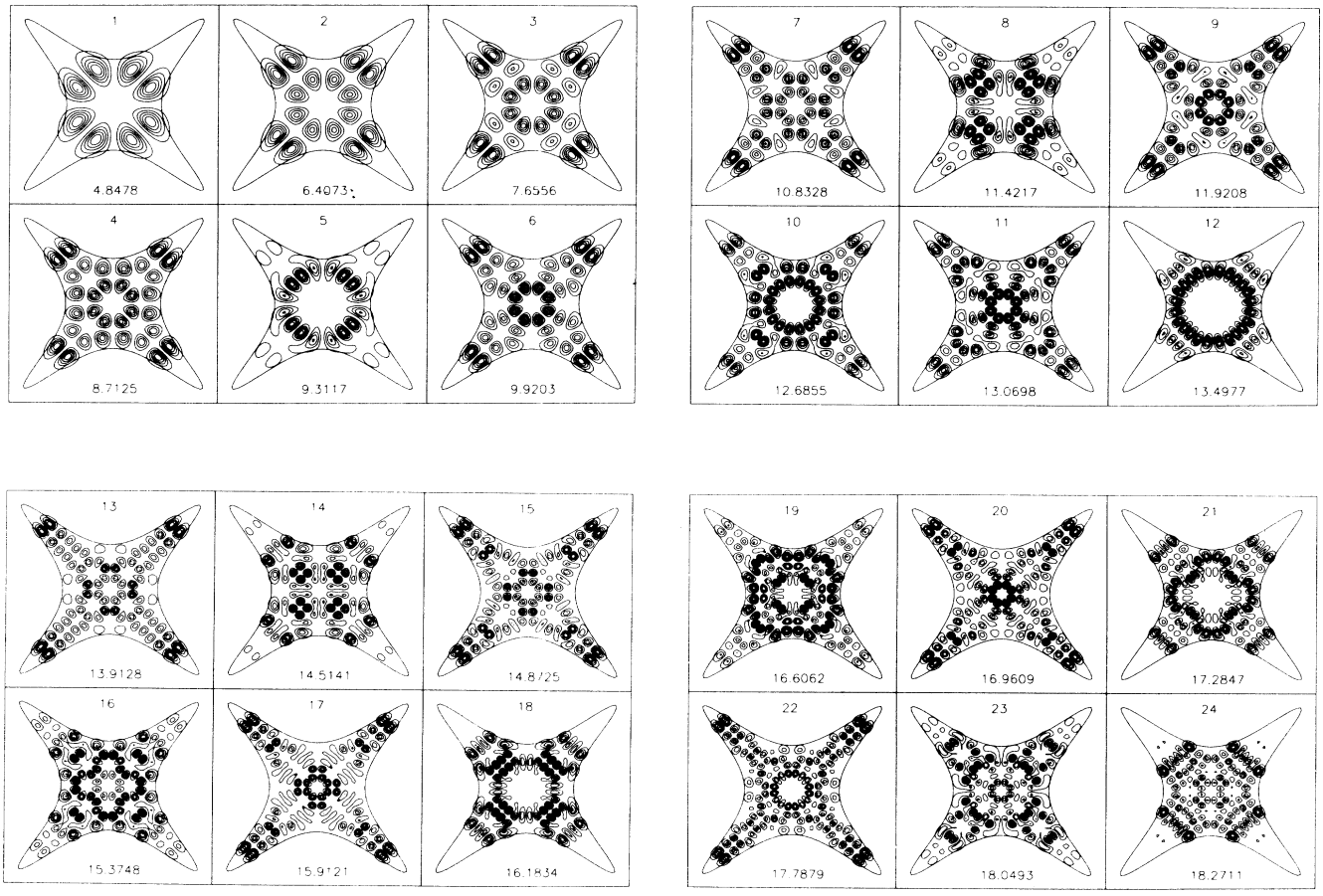

FIG. 4. Densities of the lowest 24 eigenstates in the symmetry class A_2.

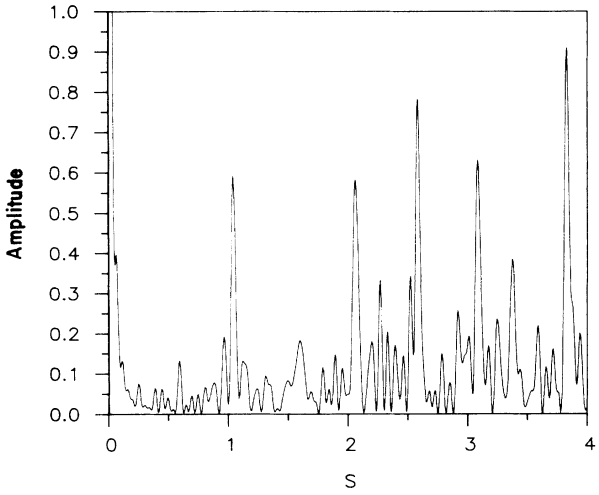

FIG. 5. Fourier transform of the density of states [Eq. (9)] for the lowest 60 states in symmetry class A_1.

batic breakup may be uniquely defined by the periodic orbits of the system. This in turn serves to shed some light on the phenomenon of scars.

Consider now the periodic orbits shown in Fig. 7(a). All these orbits lie in the vicinity of the "channel orbit" labeled 2. It is evident that with respect to all other periodic orbits in its vicinity, the channel orbit is attractive. Furthermore, inspection of Table III shows that the action of the channel orbit is greater than the action of all the neighboring orbits when taken over one traversal along the channel. Thus the channel orbit is identified as an adiabatic well. All the other periodic orbits in its vicinity may be thought of as the remnants of tori had the adiabatic approximation been exact. We will use them to construct the adiabatic Hamiltonian associated with the channel orbit. Specifically, the channel orbit defines a local orthogonal coordinate system, straight lines that are parallel and perpendicular to the orbit. The action of each one of the neighboring orbits may be split into two components $S_\parallel$ and $S_\perp$. This is shown in Fig. 11. Each periodic orbit in the channel region, at reduced energy $\varepsilon_0=1$ defines a point in the $(S_\parallel,S_\perp)$ plane. If the adiabatic approximation were exact for all these orbits then all points would lie on a single line, and this line would

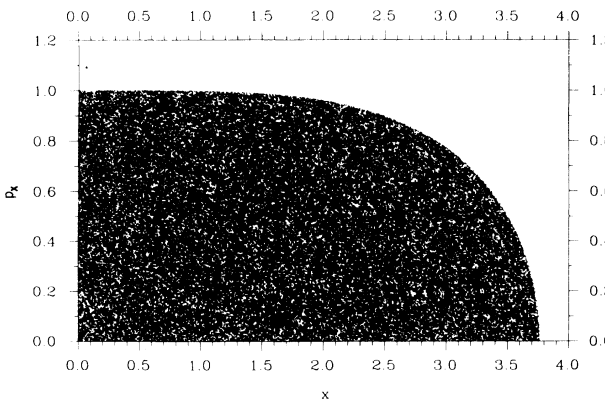

FIG. 6. Poincaré surface of section ($y=0$, $p_y>0$) for the classsical Hamiltonian (2.1) with $\beta=0.01$. Because of the symmetries only one quadrant is shown. One initial condition was iterated for 100 000 points.

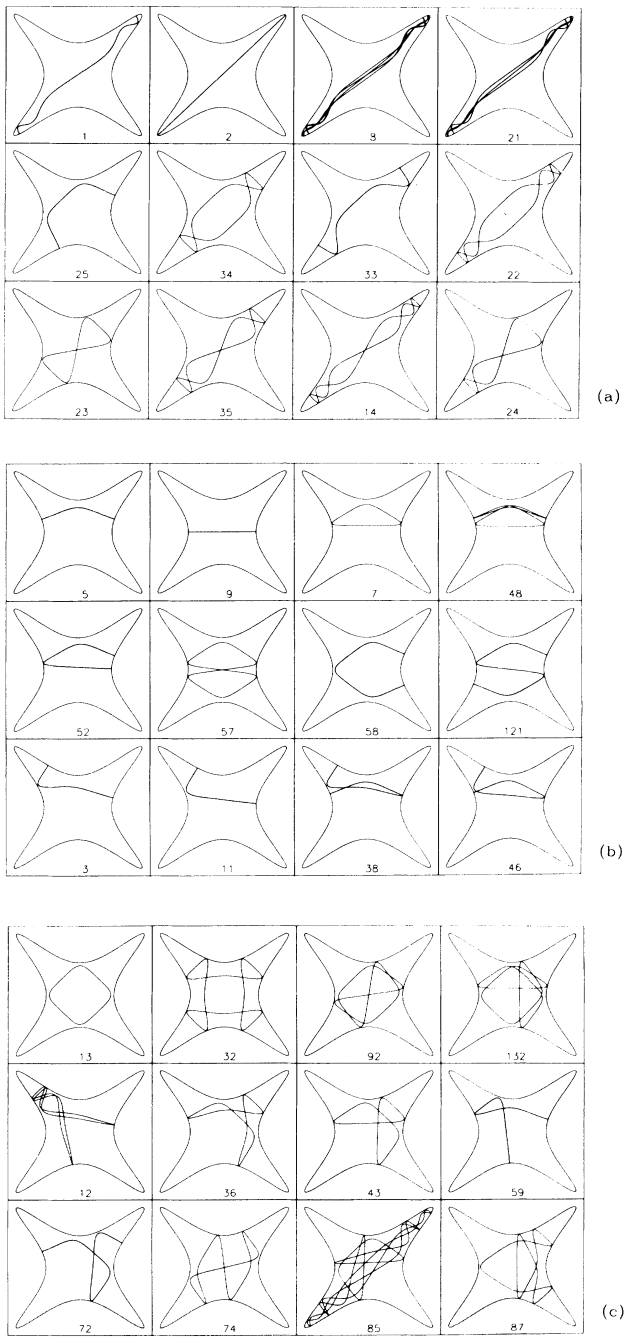

FIG. 7. Selected periodic orbits for the classical Hamiltonian with $\beta=0.01$ (and energy $E_0=\frac{1}{2}$). The first panel shows orbits that we associate with motion "along the channels;" the second panel shows orbits moving mainly "in the center," and the third shows more complicated orbits, mixing both regions. The numbers identify the orbits in Table I.

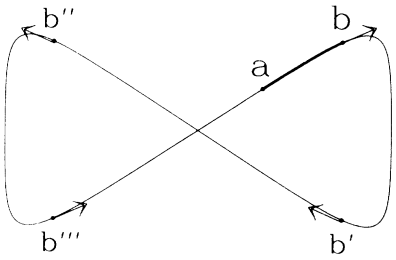

FIG. 8. Symmetry-related points on orbit no. 23 for the computation of the symmetry-reduced Green's function. The basic trajectory from a to b is indicated by a heavy line. The arrows on b and its symmetry related partners b', b'', and b''' are a reminder that the orientation has to be preserved.

define the locally integrable Hamiltonian. As can be seen from Fig. 11, although the system is not integrable one still finds that to a very good approximation the points actually do lie on a single line. Asymptotically, as the action perpendicular to the orbit vanishes, the adiabatic approximation should work best, and indeed the scatter diminishes for larger parallel actions.

One can now use a plot like Fig. 11 to reconstruct the adiabatic Hamiltonian. Denote the functional relationship between $S_\perp$ and $S_\parallel$ by

$$S_\perp = f(S_\parallel) \ . \tag{16}$$

The adiabatic Hamiltonian is a function $H(S_\perp, S_\parallel)$ and the eigenvalues are given by semiclassical quantization of the two actions

$$\varepsilon_{n,m} = H(S'_\perp = n + \alpha_\perp/4, S'_\parallel = m + \alpha_\parallel/4) \ , \tag{17}$$

where $\alpha_\parallel$ and $\alpha_\perp$ are the relevant Maslov indices. For our scale-invariant system the actions are linear in the reduced energies [cf. Eq. (5)], so we can write

$$S'_\perp = \varepsilon_{n,m} S_\perp(\varepsilon_0), \quad S'_\parallel = \varepsilon_{n,m} S_\parallel(\varepsilon_0) \ , \tag{18}$$

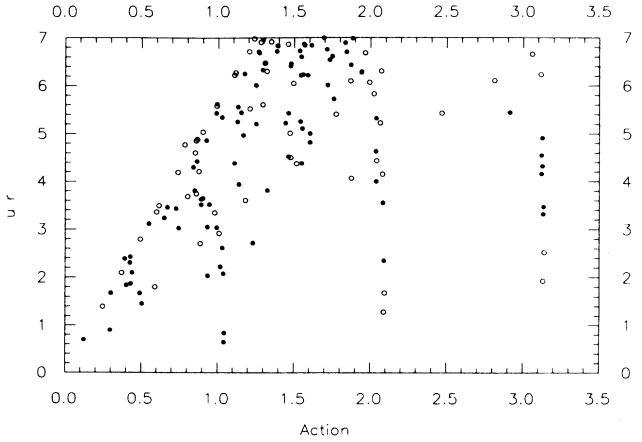

FIG. 9. All 150 periodic orbits (solid dots) and their multiple traversals (open circles) in an action-stability plane. Note the set of orbits with small eigenvalues and actions near 1.05 and 2.1.

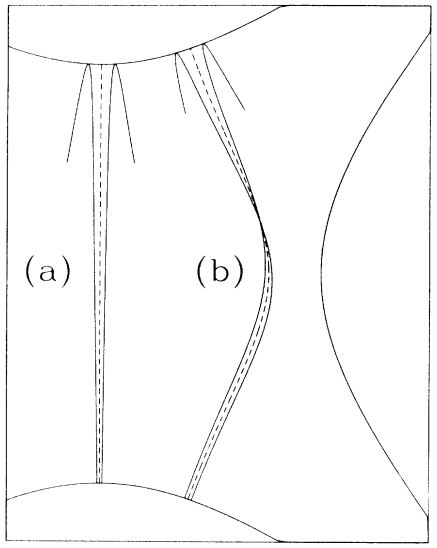

FIG. 10. Adiabatic stability of periodic orbits, illustrated using the Lyapunov unstable orbits 9 and 5. Initial conditions are taken along equienergy contours and the periodic orbit is indicated by a dashed line. (a) Orbit 9 is adiabatically unstable since orbits started nearby immediately diverge away from the periodic orbit. (b) Orbit 5 is adiabatically stable, since nearby orbits cross the periodic orbit.

where the actions with argument ε_0 also have to satisfy the restriction (16). The ratio of the two actions is fixed so that one can solve say for $S_\perp(\varepsilon_0)$ in terms of $S_\parallel(\varepsilon_0)$:

$$S_\perp^{n,m}(\varepsilon_0) = \frac{n + \alpha_\perp/4}{m + \alpha_\parallel/4} S_\parallel^{n,m}(\varepsilon_0) \ . \tag{19}$$

Using Eq. (16) one can solve for $S_\parallel^{n,m}(\varepsilon_0)$ which together with the quantization rule and Eq. (18) gives the energy.

For example, let us assume that Eq. (16) describes a linear relationship (as is indeed approximately the case in our system)

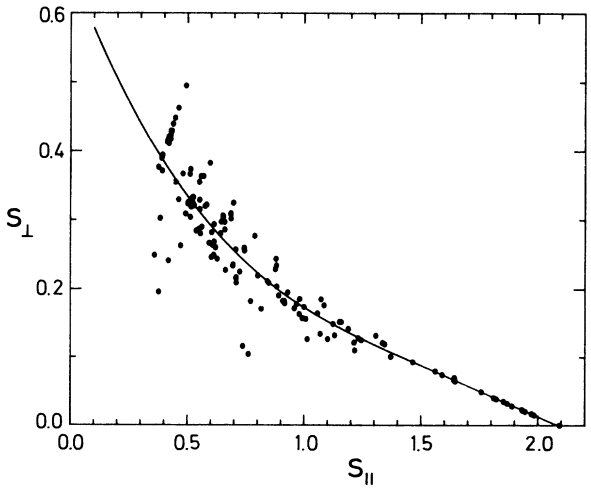

FIG. 11. Effective Hamiltonian as computed from projections of all periodic orbits.

$$S_\perp = aS_\parallel + b \ . \tag{20}$$

Replacing $S_\perp$ by (19) one can solve for $S_\parallel$. The corresponding eigenvalue now follows by demanding that $\varepsilon S_\parallel(\varepsilon_0)=(m+\alpha_\parallel/4)$. This leads to an explicit form for the energies

$$\varepsilon_{n,m} = (-a/b)(m+\alpha_\parallel/4)+(n+\alpha_\perp/4)/b \ . \tag{21}$$

Before applying this result to our system we have to deal with the symmetries. The adiabatic Hamiltonian is valid for motion confined to a domain stretched along one of the channels, with an identical approximation for the other channels obtained by a rotation of $\pi/2$. This classical degeneracy is quantum-mechanically split by tunneling. To construct A_1 and B_1 states, we need wave functions that are symmetric under reflections about both axes. This holds true for adiabatic channel states with even quantum numbers. The A_1 and B_1 states are obtained by combining these degenerate adiabatic states symmetrically or antisymmetrically with respect to the diagonals. The symmetrized states are therefore also degenerate except for tunneling corrections.

Similarly, to get A_2 and B_2 states, the adiabatic channel wave functions need to be antisymmetric with respect to reflections on both coordinate axes, so the quantum numbers are odd. Symmetric and antisymmetric combinations along the diagonals then give B_2 and A_2 states, again almost degenerate in energies. In Tables I and II we compare eigenvalues predicted from adiabatic approximation with exact scaled energies. For low quantum numbers the tunneling splitting between symmetry related pairs is rather large but it quickly decreases and becomes negligible.

Instead of comparing computed eigenvalues, one can use the numerical values of the quantum energies of all those states that scar along the channel orbit, in conjunction with Eq. (18) to obtain a direct comparison with the periodic orbits. Specifically, ordering the eigenvalues with increasing energy and quantum number, one can solve for $S_\parallel^{n,m}(\varepsilon_0)$ and $S_\perp^{n,m}(\varepsilon_0)$ to obtain from the n,m eigenvalue a point in the $(S_\parallel^{n,m}(\varepsilon_0), S_\perp^{n,m}(\varepsilon_0))$ plane. All points thus obtained may then be compared with the similar results obtained from the periodic orbits. This graphical comparison is provided in Fig. 12. The agreement between between the two panels serves to point out the quality of the adiabatic Hamiltonian we have derived.

For a more quantitative comparison, note that for $S_\parallel > 1.4$ the relationship between $S_\perp$ and $S_\parallel$ is almost linear. A least-squares fit of the 18 periodic orbits in that range gives coefficients $\alpha = -0.150\,93$, $b = 0.314\,47$, and a regression coefficient of $r = -0.9992$. For the actions from 26 eigenvalues with $S_\parallel > 1.6$ one finds $a = -0.150\,97$ and $b = 0.314\,78$, with $r = -0.9989$. Again, very good agreement is found.

For the A_1 and B_1 states with their low perpendicular excitation, the linear approximation works reasonably well even for the ground state. However, for the A_2 and B_2 states and all other states with higher excitations, the linear approximation holds for higher-lying states only [e.g., if the linear approximation is used for $S_\parallel > 1.4$, then one needs to have $\varepsilon > 4.75$ for quantum numbers $(0,m)$ in the A_1, B_1 pair and $\varepsilon > 14.5$ for quantum numbers $(1,m)$ in the B_2, A_2 pair]. One can improve on that in order to get lower eigenvalues by fitting a cubic polynomial to the actions. Energies obtained in this manner are marked by an asterisk in Tables I and II.

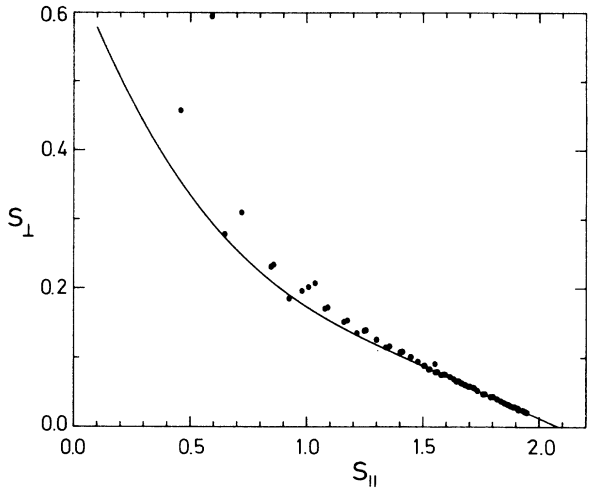

FIG. 12. Effective Hamiltonian as determined from the eigenstates identified as being scarred along the axes.

The careful reader will notice that the energy of B_1 states is not always higher than the energy for the A_1 states, as one would expect if the adiabatic approximation were exact. In fact, other states can mix in (see the nice analysis of Davis[51]) and thus invert the energy difference. Mixing in of other states also explains the rather large deviations between predicted and exact energies for the group of state nos. 22 and 23 of A_2 and nos. 25 and 26 of B_2 (see Table II). From Fig. 4 one would identify no. 22 as scarred along the channel and not no. 23 as indicated in our table. To identify whether another state mixes in, we show in Fig. 13 the densities for $|\psi_{22}\pm\psi_{23}|^2$. The figure reveals an adiabatic channel state and another state that interact. A similar figure was found for the states of the B_2 symmetry. Interestingly, the average energy of all four states is 17.876 in reasonable agreement with the predicted semiclassical energy of 17.969. This correspondence implies that at this energy there are two different adiabatic states with the same energy. All of these four

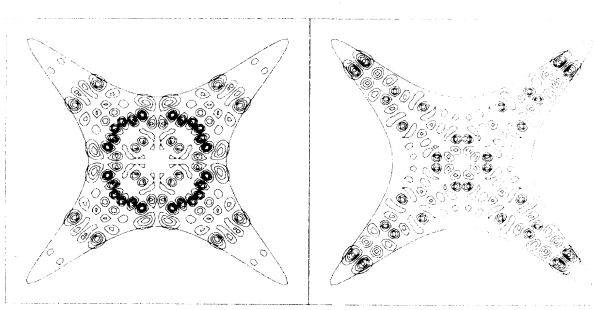

FIG. 13. Superposition of states 22 and 23 of the A_2 symmetry. The densities of the added (left) and subtracted (right) states reveal an adiabatic channel state and another state.

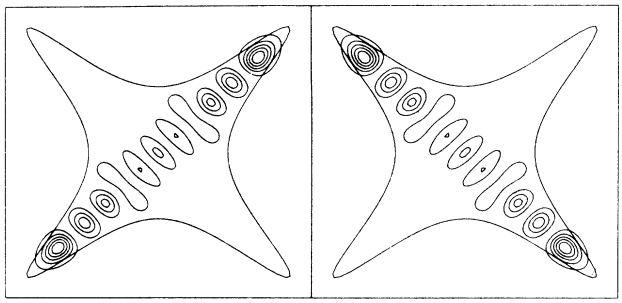

FIG. 14. Superposition of state 7 of the A_1 symmetry and 5 of the B_1 symmetry. The densities of the added (left) and subtracted (right) states reveal the underlying adiabatic state, concentrated along the channel and having quantum numbers $m=10$ and $n=0$.

states interact weakly to give a quartet of states. We expect that as the density of states increases, that is as one goes up in energy, such "accidental degeneracies" will stop becoming accidental, and one will see that more and more adiabatic states interact. In some sense this amounts to having scars of different periodic orbits in the same wave function.

Another check of our analysis is the distribution of nodal lines. However, one has to beware of effects of symmetrization. For instance, state 7 of the A_1 states seems to have ten nodal lines along the channel whereas state 5 of the B_1 sequence, predicted to be almost degenerate with the preceding state by our analysis, seems to have only nine. In Fig. 14 we demonstrate that by adding and subtracting the two states one can recover adiabatic states with the right number of nodal lines along the channels. Superposition of states also reveals higher excitations perpendicular to the orbit. An example is shown in Fig. 15.

An analysis of the predicted eigenvalues, the exact quantal eigenvalues, and the wave functions, shows that there is a one-to-one correspondence between all eigenvalues that are associated with adiabatic quantization and wave functions that scar along the channels. Indeed, the adiabatic analysis covers all of those wavefunctions that scar along the channels. The adiabatic analysis could thus be used not only to predict the eigenvalues of a subset of states but also the dominant contribution to the wave functions.

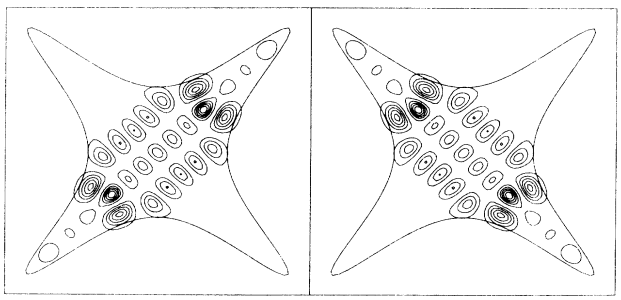

FIG. 15. Superposition of states 11 (A_1) and 9 (B_1). The dominant contribution to this state is an adiabatic state with quantum numbers $m=6$ and $n=2$.

IV. DISCUSSION

In the preceding section we presented a detailed study of all low-lying eigenstates of the quartic oscillator. On the basis of an adiabatic breakup we could assign quantum numbers to all states concentrated along the channels, thus also explaining the scars. This success raises several questions. (a) What limits the accuracy and predictive power of the method? (b) How critically does it depend on the adiabatic breakup? (c) Can it be generalized to other orbits, to other systems? We will address these questions in turn.

From the quantization scheme outlined in the preceding section, it is clear that the accuracy of the prediction for the eigenvalue is given by the scatter of points in Fig. 11. This scatter is rather large if the two actions are comparable, but it decreases as $S_\perp/S_\parallel \to 0$, i.e., as the parallel action becomes much larger than the perpendicular action. Numerically, this scatter is <0.002 for actions $S_\parallel > 1.6$. At a reduced energy of 25 this implies an uncertainty of about 0.05, which is still smaller than the average spacing $\Delta\varepsilon \approx 0.178$ estimated from the classical density of states [cf. Eq. (6)]. However, for higher energies this uncertainty will become larger than the mean spacing at which point the predictive power for a single eigenstate will be lost.

Our method of quantization also fails, if the perpendicular excitation is too high, for then one is in the regime of small $S_\parallel(\varepsilon_0)$ where the scatter is large. For instance, requiring $S_\parallel(\varepsilon_0) > 1.6$ as in the preceding section leads to an estimate $\varepsilon > 24.2$ for states with quantum numbers $(2,m)$ (A_1, B_1 states). But already at lower energies higher perpendicular excitations become noticeable, as illustrated in Fig. 15.

Turning to the dependence on the coordinates, we note that if the system were integrable, then all points would lie on a line and any (complete) coordinate system would be equivalent. This is the invariance of integrable systems under canonical coordinate changes. Our method *is* coordinate dependent. We need to specify the coordinate axis to compute the perpendicular or parallel actions; this is done by identifying the adiabatic well around which the orbits are organized. Then we need to count the number of excitations in both coordinates and derive from that the actions per period. Once this is done one can again imagine invariance of these actions under canonical changes of coordinates, however, for the computation the proper choice of coordinates is crucial.

Inspection of the wave functions plotted in Figs. 1–4 shows that scars may be found also in the central region of configuration space. For example, the A_1 states 13,20, and 50 are highly localized and one could imagine that they arise from an adiabatic breakup around periodic orbits 5 or 13. Similar scarred states may be found in other symmetries. A quantitative estimate for these states (as well as for states with E symmetry) will, we hope, be presented elsewhere. It is, though, clear that the same limitations found for the channel orbit will remain. If the

scatter in action space is too large, or the density of states too high, one will not be able to make accurate predictions for single eigenstates. Since in principle different adiabatic breakups give different Hamiltonians, one can imagine a situation where at high energy states from the different Hamiltonians overlap. At this point, one will find quantum states that scar along two or more periodic orbits as seems to be the case for the scars in the stadium problem.[27,28]

Here, we note that this method should also be applicable to analysis of the quadratic Zeeman effect in strong magnetic fields. The effective Hamiltonian in semiparabolic coordinates is qualitatively similar to the quartic oscillator (1): there are channels along the coordinate axes. An adiabatic analysis of the periodic orbits for the quadratic Zeeman system is in progress.

It is interesting to compare our findings with other periodic orbit quantization schemes. As discussed in several places in the literature (see, e.g., Miller[52] or Voros[53]) every primitive (i.e., nonrepeated) periodic orbit formally leads to a pole in the density of states at

$$S_\gamma \varepsilon = (m + \nu_\gamma \pi/4)\hbar + i u_\gamma (n + \tfrac{1}{2})\hbar \ . \tag{22}$$

If the orbit is unstable (u_γ real), then the corresponding energies are complex and interpreted as resonances with location given by the real part of the energy and a width given by the imaginary part. This directly links the stability of the periodic orbit and the uncertainty in the location of the eigenvalue (i.e., the width of the resonance). In our approach, the uncertainty in the location of the energy is associated with the scatter of points in the $(S_\parallel, S_\perp)$ plane. This scatter is not known to be directly related to u_γ. In other words, the two methods would predict different widths.

We also note that the periodic orbit quantization [Eq. (22)] has difficulty in predicting the nonlinear increase in the effective Hamiltonian for small $S_\parallel$. The quantization rule (22) is intrinsically linear (for the scaled variables) and thus the nonlinear increase could come only from a collective effect in the superposition of many orbits.

Our results may be interpreted as an effective resummation of the periodic orbit formula in the following sense. For an integrable system both the torus quantization rule and the periodic orbit formula lead to the same density of states (see Berry and Tabor[44,45]), but as demonstrated recently by Keating and Berry,[54] the latter generally requires knowledge of all periodic orbits. The classical Hamiltonian implicitly contains the information about all periodic orbits and is thus the more efficient method of quantization. Our method maps every orbit of the full system onto a periodic orbit of an integrable system and in this sense introduces an effective Hamiltonian. This mapping is many to one, since there are vastly more isolated periodic orbits in a chaotic system than in an integrable one. But the numerical results show that the actions of the true orbits do not differ too much from the approximate actions. In particular, as long as the deviations are smaller than $\hbar$, one would expect quantum mechanics to be insensitive to these changes.

Insensitivity of quantum mechanics to classical effects smaller than $\hbar$ is also the reason for the success of quantization methods based on semiclassical quantization of truncated classical perturbation series (see, e.g., the work on truncated Birkhoff-Gustavson normal forms beginning with Swimm and Delos[55]). However, these are usually considered in regions where the stochastic layers are an insignificant part of phase space. More recently Reinhardt and Dana[56,57] (see also Izraelev and Sokolov[58,59] for asimilar ansatz) have studied the adiabaticity of classical constant action perturbation series for the standard map and they find them to provide good adiabatic invariants even for strong chaos in the classical map. It remains to be seen whether one can use such a method also for the quartic system.

ACKNOWLEDGMENTS

We would like to thank J. M. Gomez Llorente, J. Reichl, P. H. Richter, and D. Wintgen for helpful discussions. This work has been generously supported by grants from the U.S. Israel Binational Science Foundation and the Minerva Foundation.

[1]M. V. Berry, in *Chaotic Behavior in Deterministic Systems*, edited by G. Iooss, R. H. G. Helleman, and R. Stora (North-Holland, Amsterdam, 1983), p. 171ff.
[2]B. Eckhardt, Phys. Rep. **163**, 205 (1988).
[3]M. V. Berry and M. Tabor, Proc. R. Soc. London, Ser. A **356**, 375 (1977).
[4]G. M. Zaslavski, Zh. Eksp. Teor. Fiz. **73**, 2089 (1977) [Sov. Phys.—JETP **46**, 1094 (1977)].
[5]S. W. McDonald and A. N. Kaufman, Phys. Rev. Lett. **42**, 1189 (1979).
[6]O. Bohigas, M. J. Giannoni, and C. Schmit, Phys. Rev. Lett. **52**, 1 (1984).
[7]O. Bohigas, M. J. Giannoni, and C. Schmit, J. Phys. Lett. (Paris) **45**, 1015 (1984).
[8]O. Bohigas and M. J. Giannoni, in *Mathematical and Computational Methods in Nuclear Physics*, edited by J. S. Dehesa *et al.* (Springer, Berlin, 1984), p. 1.
[9]M. V. Berry and M. Robnik, J. Phys. A **19**, 649 (1986).
[10]M. Robnik and M. V. Berry, J. Phys. A **19**, 669 (1986).
[11]R. Scharf, B. Dietz, M. Kuś, F. Haake, and M. V. Berry, Europhys. Lett. **5**, 383 (1988).
[12]M. C. Gutzwiller, J. Math. Phys. **8**, 1979 (1967).
[13]M. C. Gutzwiller, J. Math. Phys. **10**, 1004 (1969).
[14]M. C. Gutzwiller, J. Math. Phys. **11**, 1791 (1970).
[15]M. C. Gutzwiller, J. Math. Phys. **12**, 343 (1971).
[16]M. C. Gutzwiller, Physica D **5**, 183 (1982).
[17]M. C. Gutzwiller, J. Phys. Chem. **92**, 3154 (1988).
[18]A. Holle, G. Wiebusch, J. Main, B. Hager, H. Rottke, and K. H. Welge, Phys. Rev. Lett. **56**, 2594 (1986).
[19]J. Main, G. Wiebusch, A. Holle, and K. H. Welge, Phys. Rev. Lett. **57**, 2789 (1986).
[20]A. Holle, G. Wiebusch, J. Main, K. H. Welge, G. Zeller, G. Wunner, T. Ertl, and H. Ruder, Z. Phys. D **5**, 279 (1987).
[21]J. Main, G. Wiebusch, A. Holle, and K. H. Welge, Z. Phys. D **6**, 295 (1987).
[22]A. Holle, J. Main, G. Wiebusch, H. Rottke, and K. H. Welge,

Phys. Rev. Lett. **61**, 161 (1988).
[23]D. Wintgen, Phys., Rev. Lett. **58**, 1589 (1987).
[24]D. Wintgen and H. Friedrich, Phys. Rev. A **36**, 131 (1987).
[25]D. Wintgen, Phys. Rev. Lett. **61**, 1803 (1988).
[26]H. S. Taylor, J. Zakrzewski, and S. Saini, Chem. Phys. Lett. **145**, 555 (1988).
[27]E. Heller, Phys. Rev. Lett. **53**, 1515 (1984).
[28]E. Heller, in *Quantum Chaos and Statistical Nuclear Physics,* edited by T. H. Seligman and H. Nishioka (Springer, Berlin, 1983), p. 162.
[29]E. B. Bogomolny, Pis'ma Zh. Eksp. Teor. Fiz. **44**, 436 (1986) [JETP Lett. **44**, 561 (1986)].
[30]E. B. Bogomolny, Physica D **31**, 169 (1988).
[31]E. Pollak, Chem. Phys. **61**, 305 (1981).
[32]A. Carnegie and I. C. Percival, J. Phys. A **17**, 801 (1984).
[33]S. G. Mantinyan, G. K. Savvidy, and N. G. Ter-Arutyunyuan-Savvidy Zh. Eksp. Teor. Fiz. **80**, 830 (1981) [Sov. Phys.—JETP **53**, 421 (1981)].
[34]G. K. Savvidy, Nucl. Phys. **B246**, 302 (1984).
[35]H. D. Meyer, J. Chem. Phys. **84**, 3147 (1986).
[36]M. Baranger and K. T. R. Davies, Ann. Phys. (N.Y.) **177**, 330 (1987).
[37]M. A. M. DeAguiar, C. P. Malta, M. Baranger, and K. T. R. Davies, Ann. Phys. (N.Y.) **180**, 167 (1987).
[38]B. E. would like to thank J. Reichl for this important suggestion.
[39]R. DeVogelaere, in *Contributions to the Theory of Nonlinear Oscillations,* edited by S. Lefschetz (Princeton University Press, Princeton, 1958), pp. 54–84.
[40]E. Pollak, M. S. Child, and P. Pechukas, J. Chem. Phys. **72**, 1669 (1980).
[41]M. Hénon, Physica D **5**, 412 (1982).
[42]M. V. Berry and K. E. Mount, Rep. Prog. Phys. **35**, 315 (1972).
[43]M. Tabor, Physica D **6**, 195 (1983).
[44]M. V. Berry and M. Tabor, Proc. R. Soc. London, Ser. A **392**, 101 (1976).
[45]M. V. Berry and M. Tabor, J. Phys. A **10**, 371 (1977).
[46]W. H. Miller, J. Chem. Phys. **48**, 1651 (1968).
[47]E. Pollak, J. Chem. Phys. **74**, 5586 (1981).
[48]E. Pollak, in *Theory of Chemical Reaction Dynamics,* edited by M. Baer (CRC, Boca Raton, 1985), Vol. 3., p. 123.
[49]M. Shapiro, R. D. Taylor, and P. Brumer, Chem. Phys. Lett. **106**, 325 (1984).
[50]Y. Y. Bai, G. Hose, K. Stefánski, and H. S. Taylor, Phys. Rev. A **31**, 2821 (1985).
[51]M. Davis, J. Phys. Chem. **92**, 3124 (1988).
[52]W. H. Miller, J. Chem. Phys. **63**, 996 (1975).
[53]A. Voros, J. Phys. A **21**, 685 (1988).
[54]J. P. Keating and M. V. Berry, J. Phys. A **20**, L1139 (1987).
[55]R. T. Swimm and J. B. Delos, J. Chem. Phys. **71**, 1706 (1979).
[56]W. P. Reinhardt and I. Dana, Proc. R. Soc. London, Ser. A **413**, 157 (1987).
[57]I. Dana and W. P. Reinhardt, Physica D **28**, 115 (1987).
[58]F. M. Izraelev and V. V. Sokolov, Phys. Lett. **112A**, 254 (1985).
[59]V. V. Sokolov, Theor. Math. Phys. **67**, 464 (1986).